AGU PUBLICATIONS

JGR

Journal of Geophysical Research: Solid Earth

RESEARCH ARTICLE

10.1002/2016JB013744

Key Points:

- The paper presents a comprehensive laboratory investigation of the THM behavior of a low-permeability argillaceous rock
- The novel investigation of the thermally induced pore pressure rise in a fluid-filled cavity is used to validate a THM model
- The experiments are used to assess the predictive capabilities of a computational model

Correspondence to:
A. P. S. Selvadurai,
patrick.selvadurai@mcgill.ca

Citation:
Selvadurai, A. P. S., and M. Najari (2017), The thermo-hydro-mechanical behavior of the argillaceous Cobourg Limestone, *J. Geophys. Res. Solid Earth*, *122*, doi:10.1002/2016JB013744.

Received 31 MAY 2016
Accepted 23 APR 2017
Accepted article online 27 APR 2017

The thermo-hydro-mechanical behavior of the argillaceous Cobourg Limestone

A. P. S. Selvadurai[1] **and M. Najari**[1]

[1]Department of Civil Engineering and Applied Mechanics, McGill University, Montréal, Quebec, Canada

Abstract The Cobourg Limestone is a low-permeability argillaceous rock that forms a part of the Paleozoic sedimentary sequence found in southern Ontario, Canada. The limestone has a heterogeneous fabric consisting of nodular regions of calcite and dolomite and argillaceous partings of a similar composition but with a low clay content, which gives the appearance of nominal stratifications. The thermo-hydro-mechanical (THM) behavior of the rock is of interest to the proposals for using sedimentary formations as candidate rocks for siting deep geological repositories for the storage of heat-emitting nuclear fuel waste. The paper presents the results of experiments where THM processes were initiated in an intact cylindrical sample of the Cobourg Limestone containing a central cylindrical fluid-filled cavity. Biot's classical theory of poroelasticity, extended to include thermal effects, is used to examine the THM response of the fluid cavity due to boundary heating of the cylinder. The rise and decay of thermally induced cavity fluid pressure is used to examine the applicability of the THM modeling. The experiments were conducted on cylindrical samples of the Cobourg Limestone with their axes either along or normal to the nominal planes of the argillaceous partings.

Plain Language Summary The thermo-poroelastic behavior of heterogeneous geological media is of interest to the engineering geosciences and geotechnique. The topic of geologic disposal of heat-emitting radioactive waste is one area of application where these multiphysics concepts are used to validate the feasibility of the disposal scheme and in particular the integrity of fluid-saturated geologic media under the action of heat. Further applications include geothermal energy extraction, geologic disposal of greenhouse gases in fluidized forms, and the loading of repository locations by glaciers. The general area of heat-induced pore fluid generation is also of interest to the geological phenomena encountered in earthquake fault zones. The coupled interaction of mechanical deformations and the pore fluids under the action of heating was examined through the development of a laboratory simulation complemented by computational modeling. The laboratory simulations performed in connection with this research provide a canonical experiment that can be used to examine multiphysics processes.

1. Introduction

Deep geologic disposal in stable host rock formations represents the most widely advocated method for the storage of *heat-emitting long-lived nuclear fuel waste*. The availability of geological settings that are considered stable for timescales relevant to sequestration is recognized as an important aspect for developing a reliable disposal strategy. The candidate geologic settings for siting high-level nuclear repositories vary from country to country; granitic rock formations have been considered by countries such as Canada, Japan, Sweden, and Switzerland; clay deposits have been considered by Belgium, France, and Switzerland; porous tuffs have been examined by the U.S.; salt formations are also favored by several European countries including Germany; the potential sites favored by the UK have complex geological settings consisting of Ordovician volcanic rocks overlain by a sequence of Carboniferous Limestone, Permian Breccia, and Triassic sandstones. Attention has also been given to argillaceous rocks in France and Switzerland. An example is the Torcian shale encountered in the Tournemire Underground Research Laboratory site and the Callovo-Oxfordian argillite encountered at the Bure site in France. The Opalinus clay, of Jurassic origin, is a moderately overconsolidated marine claystone of the Mesozoic-Tertiary sedimentary Molasse Basin of northern Switzerland. This geologic formation has been extensively studied to examine its suitability as a geologic repository for high-level nuclear fuel waste. In the Canadian context, the favored geological setting for deep geological disposal of the heat-emitting high-level nuclear fuel waste has been the granitic rocks of the Canadian Shield. More recently, Canadian efforts have been directed to argillaceous formations of southern Ontario as possible sites for the construction of a deep ground repository [*Mazurek*, 2004; *Ontario Power Generation* (*OPG*), 2008; *Neuzil*, 2011; *Neuzil and Provost*, 2014]. The

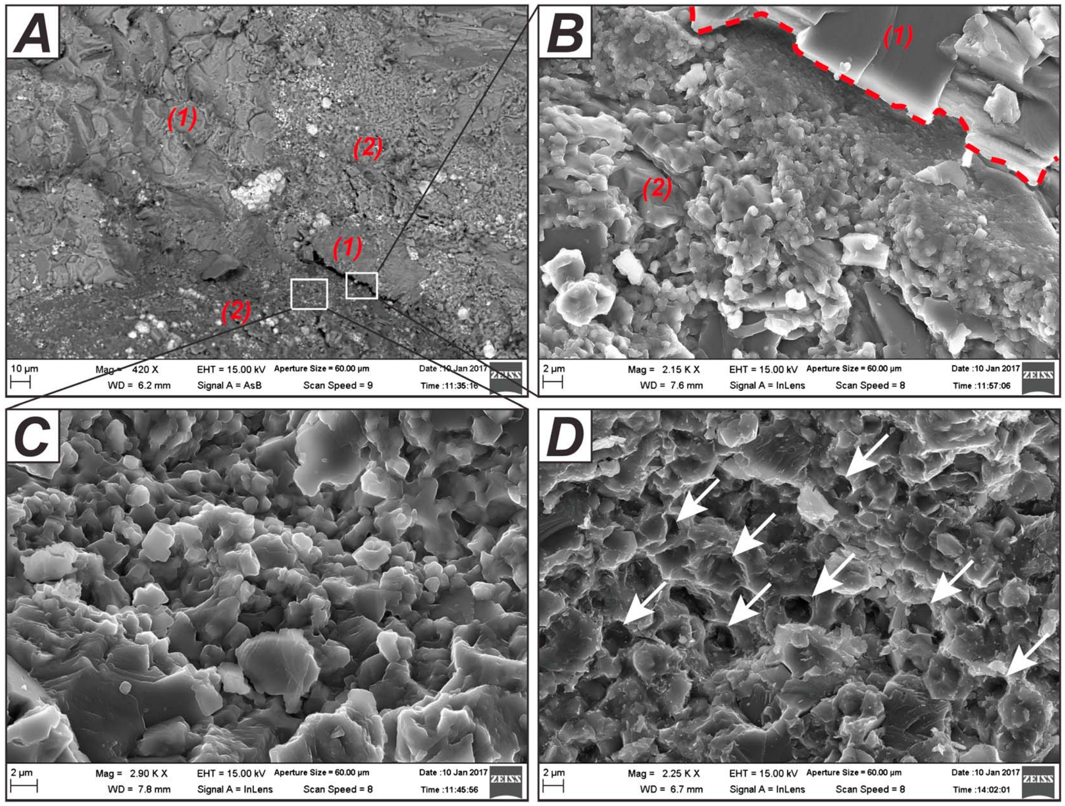

Figure 1. (a) Cobourg Limestone layout with boundary between the two microtexture phases: (1) the main calcite phase and (2) the argillaceous phase. (b) Close-up of the microtexture boundary of Figure 1a. (c) Matrix layout of the argillaceous area. (d) Well-developed microporosity network in the argillaceous part.

interest in argillaceous rocks stems from observations that, in the intact state, they have very low permeability ($K \sim (10^{-19}$ to $10^{-21})$ m^2), which is a desirable characteristic that could minimize groundwater movement in a repository setting. In certain instances, argillaceous limestones are known to possess self-healing properties that could offer additional benefits for minimizing fluid transport through the rock in situations where damage can result from alteration in the stress states either due to construction of the repository facilities or due to radiogenic heating. In all endeavors involving the deep geologic disposal of heat-emitting nuclear waste, the influence of radiogenic heating on the thermo-hydro-mechanical (THM) behavior of the repository rock mass is one of the important factors that will determine long-term effectiveness and integrity of the disposal facility.

In this paper, we present a laboratory investigation of the THM behavior of the Cobourg Limestone obtained from rock outcrops in southern Ontario. Experimental research programs that previously examined the hydraulic and hydromechanical characteristics of Cobourg Limestone [*Selvadurai et al.*, 2011; *Selvadurai and Najari*, 2016] are complemented by computational approaches that model nonisothermal poromechanics [*Selvadurai and Suvorov*, 2016]. These developments are used to examine an experiment involving the boundary heating of a cylindrical sample of the Cobourg Limestone containing a fluid-filled, axisymmetrically positioned surficial cylindrical cavity. The experimental arrangement is meant to provide a canonical example that can be used to validate a THM approach; this can eventually be used to examine the THM behavior of a high-level nuclear waste repository.

2. The THM Experiments

Comprehensive accounts of the geological setting of the Cobourg Limestone formation are given by *Mazurek* [2004] and *Neuzil and Provost* [2014]. The geologic formations are nearly horizontally stratified, and the approximately 45 m thick Middle Ordovician Cobourg formation is located about 630 m below ground

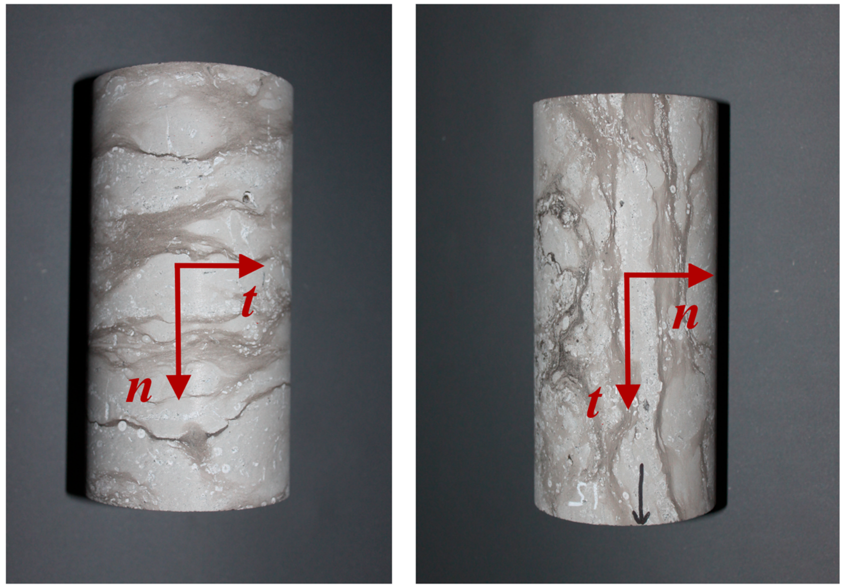

Figure 2. Nominal stratification in cylindrical (85 mm diameter) samples of the Cobourg Limestone.

level. The Cobourg formation is overlain by Upper Ordovician siltstone and gray shale extending to a depth of 200 m and underlain by Argillaceous Limestone and gray shale, approximately 150 m thick. The entire sequence of Paleozoic rocks rests on a Pre-Cambrian Granitic Gneiss basement rock [*OPG*, 2008].

2.1. Test Specimens

The Cobourg Limestone used in the experimental research was cored from large block samples obtained from the Saint Mary's Quarry in Bowmanville, ON. The blocks were cut to cuboidal sizes measuring approximately 0.5 m × 1.0 m × 0.75 m and cored to produce the cylindrical samples used in the experimental research. Cobourg Limestone displays heterogeneity resulting from the interspersed fabric of a calcite, dolomite-rich light gray nodular limestone separated by argillaceous partings. There is some visual evidence of a nominal plane of stratification, but this can vary from sample to sample depending on the spatial arrangement of the fabric. In terms of mineralogy, the light gray nodular limestone is composed of carbonates (84%) consisting of calcite (85% to 91%) and dolomite (5%) and quartz (8%) with traces of clays (0.3%). The argillaceous partings, the darker gray limestone, on the other hand contain carbonates (66%) consisting of calcite (51%) and dolomite (16%) and quartz (22%), with a clay content of 2.4% (Illite, Kaolinite, and a trace of Montmorillonite). The porosity (n) of the Cobourg Limestone exhibits variability consistent with the heterogeneity of the rock. The porosity obtained from a saturation sequence gave a value of $n = 0.006$, which can be compared with the value of $n = 0.015$ obtained using a vacuum water saturation technique by *Selvadurai et al.* [2011]. Recently, Mercury Intrusion Porosimetry was also used to examine the porosity of four samples of Cobourg Limestone (see the KCL LINK referred in the Acknowledgements). The porosities were estimated to vary within 0.0061 to 0.0065, which is consistent with the results obtained from the saturation sequence. The median pore radius was measured to be between 0.0432 μm and 0.3294 μm. The micrograph image of a Cobourg Limestone sample is shown in Figure 1. The photographs show that the micropores and microchannels are predominantly located in the argillaceous partings (dark gray species). Cylindrical samples of the Cobourg Limestone measuring 150 mm in diameter and 278 mm long were cored both normal to and along the nominal bedding plane and, at the scale of the cylinders, displayed evidence of nominal stratifications (Figure 2). CT scans of the cores (Figure 3) also point to the persistence of the fabric. It must, however, be emphasized that these observations are sample and site specific.

Diamond tipped corers with an internal diameter of 150 mm were used to extract the large-diameter cores, giving a smooth cylindrical surface; the plane ends of the cores were ground parallel to ensure that any applied axial loads resulted in uniform axial stresses. A cylindrical cavity with a flat base, measuring 26 mm in diameter and 139 mm in depth, was drilled along the axis of the cylinder. The cavity was drilled to a

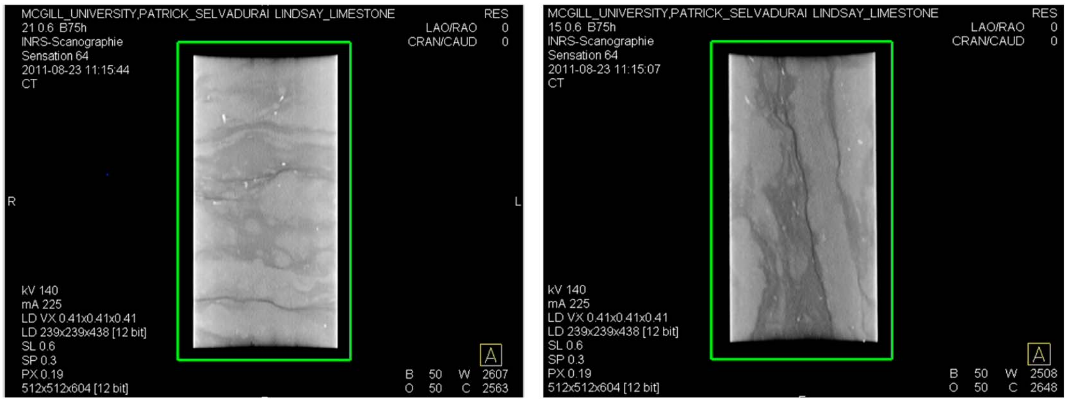

Figure 3. CT Scans of the Cobourg Limestone samples cored normal to and along the nominal stratifications.

partial height of the cylinder in order to limit the surfaces that needed sealing when the cavity was filled with water. The base of the cavity was ground flat to ensure that air bubbles could not be trapped by surface tension during filling. To enable sealing of the cavity, the plane surface of the cylinder with the cavity was fitted with a stainless steel plate that contained the fixtures necessary for filling the cavity and for monitoring the fluid pressure and temperature within the cavity.

2.2. The Test Facility and Procedures

In the current experiments, the open end of the cylindrical cavity was sealed with a stainless steel plate, which was glued to the Cobourg Limestone sample using a water-resistant marine epoxy. The schematic layout of the experimental configuration for conducting both HM and THM tests is shown in Figure 4. The Cobourg Limestone sample with the epoxy-sealed fittings was first vacuum saturated for a period of 7 days to ensure that the pore space of the rock was fully saturated. The duration for the saturation process was confirmed in previous experimental investigations [*Selvadurai et al.,* 2011; *Selvadurai and Jenner,* 2013; *Selvadurai and Najari,* 2016]. The pore fluid pressures created in the sample during the application of the vacuum were allowed to dissipate for a further 7 days. The important influences of residual pore fluid pressure fields on the decay of transient pressures created during hydraulic pulse testing were discussed by *Selvadurai* [2009]. Sufficient time was therefore allowed to ensure that residual pore fluid pressures generated during the saturation process dissipated prior to the experiments. (In the current experimental arrangements, the reduction of pressures within the cavity to negligible values is a clear indication of the reduction of excess pressures within the body of the rock to a zero value.) The saturated and depressurized Cobourg Limestone sample was placed under water in a large container to ensure that the central cavity had no visible trapped air. Using submersible heaters and a circulation pump-PID controller system, the temperature of the water reservoir in the experiment (Figure 4) was maintained at a value close to the laboratory temperature (25°C). The apparatus consisted of a loading frame with a hydraulic jack that was controlled by a gas pressure-based accumulator. This feature ensured that the axial stress applied to the sample was maintained constant during the long-duration experiment. In general, thermal expansion of the Cobourg Limestone will induce additional axial stresses in the axially constrained sample.

Type K thermocouples were installed at salient locations of the Cobourg Limestone cylinder, the cavity and in the water reservoir; the thermocouple wires that passed through the fittings were sealed with marine epoxy to eliminate moisture and pressure loss. A valve was incorporated at the stainless steel sealing plate to allow water inflow, and the pressures within the fluid-filled cavity were measured using a temperature-compensated pressure transducer (1 MPa; accuracy 0.2%).

2.3. Experiments and Results

Each sample was placed in the THM testing facility shown in Figure 4 in a saturated state with the sealed central cavity filled with water. Using steady state flow tests, the permeability of each sample was measured both before and after performing the heating experiments. A precision pump was used to apply a constant pressure of 100 kPa to the fluid-filled cavity. The changes in the water flow rate required to attain a specified cavity pressure were recorded until a steady state condition was reached. The procedures used to estimate the

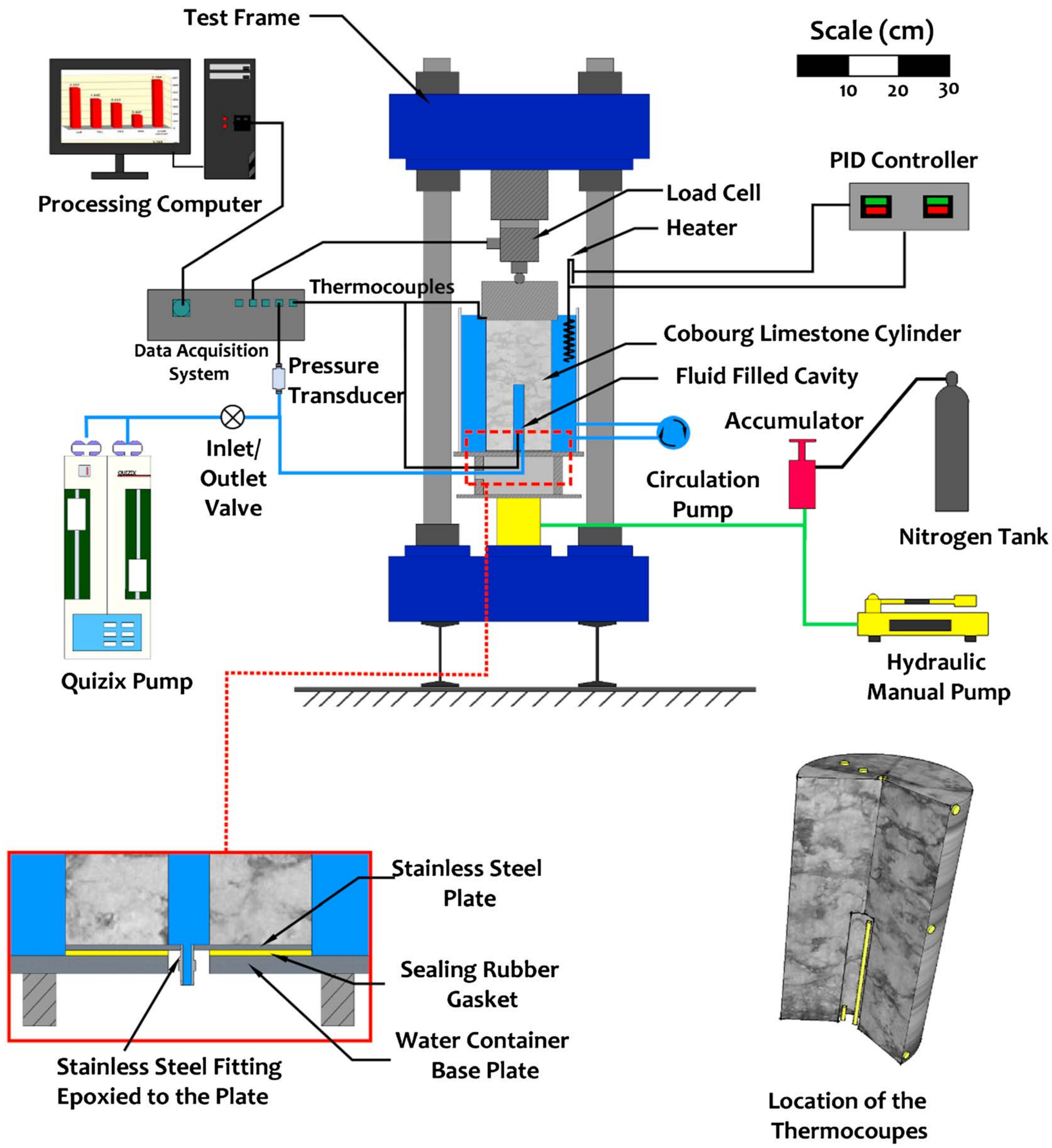

Figure 4. Schematic view of the experimental arrangement.

permeability of the samples prior to the THM tests, as well as the analytical and computational modeling techniques used in the interpretation of the results, are described in detail by *Selvadurai and Najari* [2016] and will not be repeated here. Given the geometry and the pore fluid pressure boundary conditions for each sample tested, the permeability was estimated using a computational approach. Two modeling approaches were adopted: (i) isotropic hydraulic conductivity was assumed for the rock, and the mean permeability value was estimated for each specimen, and (ii) transversely isotropic hydraulic conductivity properties were assumed for the rock, and the permeability values were estimated for each specimen along (K_H) and normal (K_V) to the nominal planes of the argillaceous partings. In order to estimate the principal permeability values for hydraulically transversely isotropic materials, at least two sets of permeability tests with independent hydraulic boundary conditions need to be conducted on each sample. An alternative approach, which was considered here, is to adopt the ratio of the principal permeabilities from the experiments performed on the Cobourg Limestone that are available in the literature. The permeability experiments performed by *Vilks and Miller* [2007] and *Gartner Lee Limited* [2008] on the Cobourg Limestone suggest an order of magnitude difference in the transverse isotropy of permeability, i.e., $(K_H/K_V) \approx 10$. Similarly, the results obtained by *Selvadurai et al.* [2011] and *Selvadurai and*

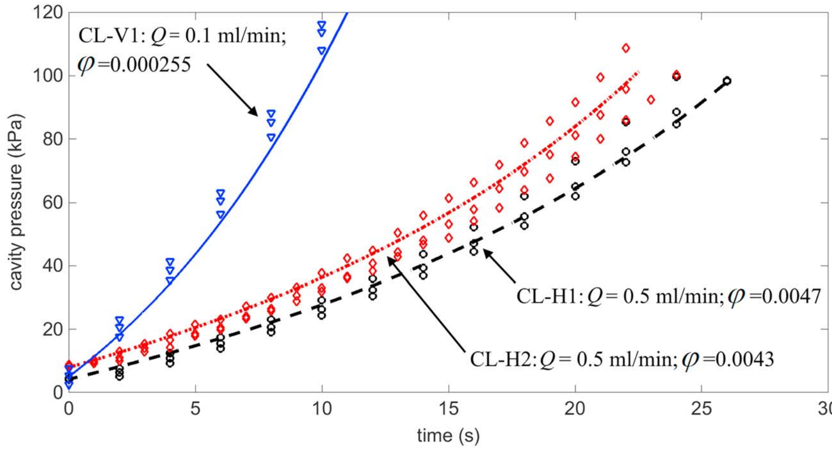

Figure 5. The pressure buildup test results (symbols) compared with the results of computational modeling (lines) for the three Cobourg Limestone samples.

Jenner [2013] point to an order of magnitude variation in the hydraulic transverse isotropy. The computational modeling therefore considers the equivalent isotropy as determined from permeability experiments and the maximum mismatch in the hydraulic conductivities indicated by $(K_H/K_V) \approx 10$. The presence of air voids in the fluid-filled cavity influences the water pressure changes in the cavity. In order to estimate the volume of air voids, a series of cavity pressure buildup tests, as proposed by *Selvadurai and Najari* [2015], were performed on each sample. The water pressure in the central cavity was increased rapidly by applying a constant flow rate; the test was performed several times to ensure repeatability of the results. The pressure buildup results were then analyzed using the computational procedure, discussed in section 3, in order to estimate the air void content in the fluid-filled central cavity. The results of the pressure buildup tests are shown in Figure 5. Table 1 presents permeability values before and after the THM experiments and the air void content in the tested samples. Thermal tests were then performed on three samples; two were cored perpendicular to the nominal stratification (samples CL-H1 and CL-H2), and one sample was cored along the orientation of the nominal stratification (sample CL-V1). The temperature on the boundary of each sample was increased in three stages: from 25°C to 40°C, from 40°C to 55°C, and from 55°C to 70°C. Each temperature increase was initiated only after sufficient time had elapsed for the dissipation of residual pressures resulting from the previous thermal excursions. The water pressure in the fluid-filled cavity and the water temperature at the two ends of the cavity obtained from the computational modeling for the three samples are compared with measured values in Figures 6–8.

3. THM Formulation

The modeling of coupled THM processes in fluid-saturated media has received extensive attention in connection with the efforts devoted to geologic disposal of heat-emitting high-level nuclear fuel waste; accounts of developments in this area are given by *Selvadurai and Nguyen* [1995], *Zimmerman* [2000], *Rutqvist et al.* [2002, 2005], *Tsang et al.* [2009], and *Tong et al.* [2010] and extensively discussed in the recent volume by *Selvadurai and Suvorov* [2016]. In the basic THM developments applicable to rocks that experience small strain behavior without initiation of damage and failure, the mechanical behavior of the porous skeleton is modeled by isotropic Hookean elasticity; also, it is noted that the mechanical response of the heterogeneous Cobourg

Table 1. The Amount of Air Void Content and the Permeability Values of the Tested Cobourg Limestone Samples

	Permeability: Before Thermal Tests			Permeability: After Thermal Tests			
	Isotropy	Transverse-Isotropy		Isotropy	Transverse-Isotropy		
Sample	K (m^2)	K_h (m^2)	K_v (m^2)	K (m^2)	K_h (m^2)	K_v (m^2)	Air Void
CL-H1	1.56×10^{-20}	1.71×10^{-20}	1.71×10^{-21}	1.36×10^{-19}	1.49×10^{-19}	1.49×10^{-20}	0.0047
CL-H2	4.9×10^{-20}	5.37×10^{-20}	5.37×10^{-21}	6.5×10^{-20}	7.12×10^{-20}	7.12×10^{-21}	0.0043
CL-V1	3.85×10^{-19}	8.44×10^{-19}	8.44×10^{-20}	1.12×10^{-18}	2.45×10^{-18}	2.45×10^{-19}	0.000255

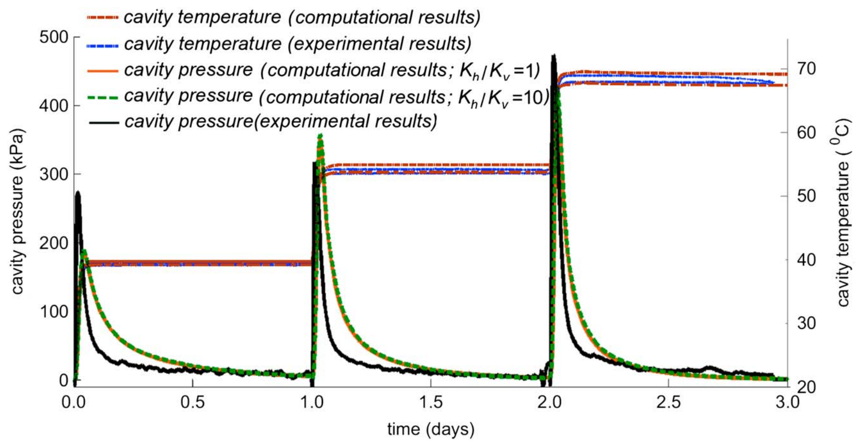

Figure 6. The results of the THM tests performed on sample CL-H1.

Limestone, despite its visible stratifications, corresponds to nominally isotropic elastic behavior where the elastic moduli in the respective orientations are not substantially different. Separate unconfined compression tests conducted on the Cobourg Limestone point to $E_H \approx 22$ GPa and $E_V \approx 25$ GPa. The fluid flow behavior in the porous medium is described by Darcy's law, and the heat transfer in the fluid-saturated porous medium is assumed to take place predominantly by heat conduction, governed by Fourier's law. The assumption of isotropic linear elastic behavior is assured when considering competent geological media similar to the intact Cobourg Limestone. However, at elevated confining stress states, rocks could exhibit elastoplastic behavior and strain hardening, as has been documented in the classical texts by *Nadai* [1963] and *Jaeger* [1965, 1972] and in the informative studies by *Farmer* [1968], *Rutter* [1974], *Baud et al.* [2000], *Vajdova et al.* [2004], *Zang and Stephansson* [2010], and *Nicolas et al.* [2016]. The coupled nature of THM processes is such that mechanical processes are assumed to be influenced by the pore fluid pressures and temperature. The flow processes are also assumed to be influenced by temperature and mechanical deformations. The heat transfer in the fluid-saturated porous medium is assumed to be by conduction only [*Carslaw and Jaeger*, 1959]. This is a widely accepted approximation for *very low permeability sparsely fractured geologic media* in which both convective and radiative components of heat transfer can be neglected in comparison to the conductive counterpart [*Selvadurai and Nguyen*, 1995]. The fact that the heat transfer by convection can be neglected if the *Peclet number* is much smaller than unity is discussed by, among others, *McTigue* [1990] and *Rehbinder* [1995]. The Peclet number (Pe) is defined by $Pe = (K\, c_p^* / \mu n\, k_c^*) p_0$, where K is the permeability, μ is the fluid viscosity, c_p^* is the effective specific heat, n is the porosity, k_c^* is the effective thermal conductivity, and p_0 is a characteristic fluid pressure. Specific estimates for the dominance of conductive heat transfer over convective heat transfer can be deduced by examining the advective term in the generalized equation of

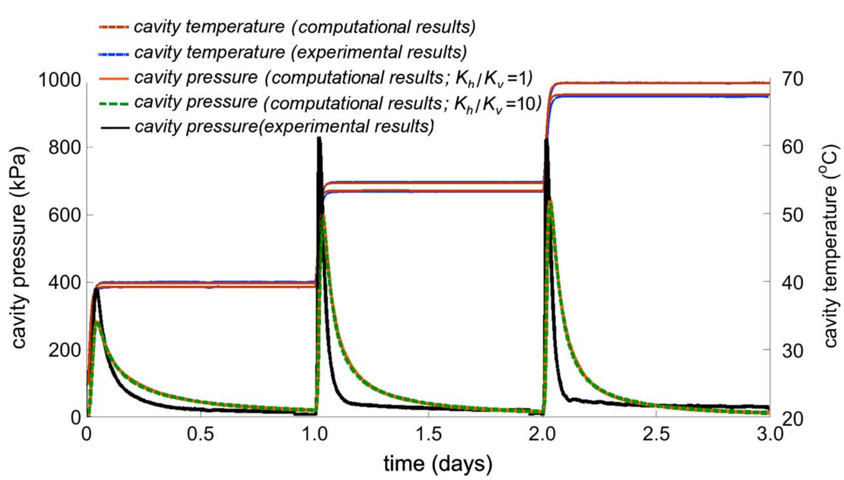

Figure 7. The results of the THM tests performed on sample CL-H2.

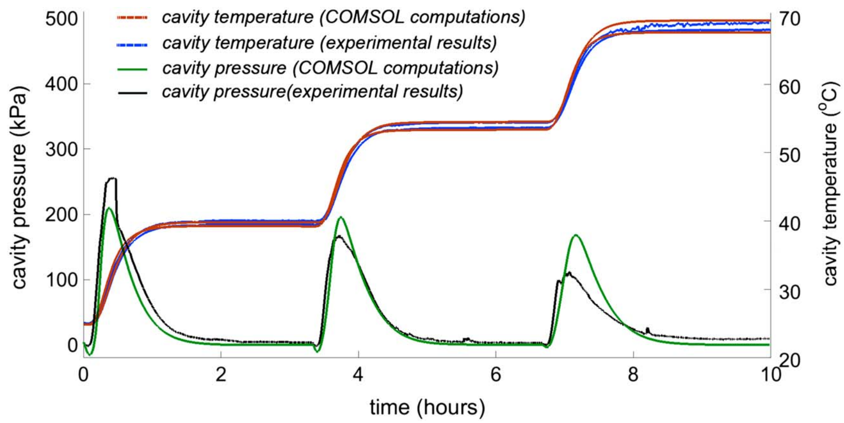

Figure 8. The results of the THM tests performed on sample CL-V1.

heat transfer in porous media [*Nield and Bejan*, 2006]. In the current studies the Peclet number satisfies the requirement $Pe << 1$ for the heating-induced pressures encountered in the cavity. We also assume that the deformation rates of the porous skeleton and rate of movement of the pore fluids through the pore space do not result in the generation of heat. The dependent variables in the formulation of the THM theory are the displacement vector $\mathbf{u}(\mathbf{x}, t)$, the pore fluid pressure $p(\mathbf{x}, t)$, and the temperature $T(\mathbf{x}, t)$, where $\mathbf{x}$ is the position vector and t is time. The resulting theory is weakly coupled, in the sense that the heat conduction in the fluid-saturated porous medium can be analyzed independently of the mechanical and fluid transport processes. The theory is an extension of the classical theory of poroelasticity [*Biot*, 1941] to include thermal effects. In order to account for influences of temperature on certain physical and mechanical properties of the permeating fluid, the coupled nonlinear partial differential equations governing THM behavior of a fluid-saturated permeable porous geomaterial can be written in the form [*Selvadurai and Nguyen*, 1995]

$$\left(K_D + \frac{G_D}{3}\right)\nabla(\nabla.\mathbf{u}) + G_D\nabla^2\mathbf{u} - \alpha\nabla p - K_D\beta_s\nabla T = \mathbf{0} \tag{1}$$

$$S\frac{\partial p}{\partial t} + \nabla.\left[-\frac{\mathrm{K}}{\mu(T)}\nabla p\right] + \alpha\frac{\partial(\nabla.\mathbf{u})}{\partial t} - [n\beta_f(T) + (\alpha - n)\beta_s]\frac{\partial T}{\partial t} = 0 \tag{2}$$

$$c^*{}_p(T)\frac{\partial T}{\partial t} - k^*{}_c\nabla^2 T = 0 \tag{3}$$

These equations take into consideration the equations of equilibrium for the porous medium, fluid mass conservation, and heat conduction in the porous medium, respectively. In (1) to (3), G_D and K_D are, respectively, the shear modulus and the bulk modulus of the porous skeleton; α is the Biot coefficient; β_s is the volumetric thermal expansion coefficient of the solid grains; S is the specific storage of the porous skeleton; $\mu(T)$ is the dynamic viscosity of water; n is the porosity; $\mathbf{K}$ is the permeability matrix; β_f is the coefficient of volumetric thermal expansion of the permeating fluid; and c_p^* and k_c^* are, respectively, the effective specific heat and effective thermal conductivity of the porous skeleton.

The specific storage term, S, is defined as

$$S = nC_w + (\alpha - n)C_s \tag{4}$$

where C_w and C_s are, respectively, the compressibility of the pore fluid and the solid grains.

Both the upper bound (*Voigt)* and lower bound (*Reuss*) estimates can be used to determine the effective specific heat capacity and effective thermal conductivity of a saturated porous medium. It is, however, observed that the *Voigt* estimate gives a result that is closer to the *Hashin and Shtrikman* [1963] improved upper bound estimate for the effective properties [see also *Christensen,* 1979]. Considering the elementary Voigt upper bound, the thermal parameters are defined by

$$k^*{}_c = nk_{cf} + (1-n)k_{cs}; \quad c^*{}_p(T) = n\rho_f(T)c_f + (1-n)\rho_s c_s \tag{5}$$

where k_{cf} and k_{cs} are thermal conductivities of the liquid phase and solid phase, respectively. Also, c_f and c_s are, respectively, the specific heat capacity of the liquid phase and the solid phase.

In the assignment of properties to the *mechanical*, *fluid transport*, and *heat conduction* processes, however, it is implicitly assumed that the properties represent the *equivalent estimates for the bulk properties*, which is a useful first approximation for the modeling of a complex heterogeneous geomaterial such as the Cobourg Limestone. More refined approaches will require the estimation of THM properties governing the individual species (i.e., the light gray nodular limestone and the darker argillaceous partings) and the interfaces between species along with the spatial distribution of the species. A consideration of the modeling of the separate species of the Cobourg Limestone is a challenging prospect both computationally and from the point of view of parameter identification. At this stage of the research program, the benefits of such a multiscale modeling approach are not entirely evident.

Special computational procedures have to be adopted for modeling THM effects in the fluid-filled cavity. Here the fluid-filled sealed cavity was modeled as a porous medium with a porosity of unity and a relatively high permeability (i.e., $K_f = 10^{-12}\,\mathrm{m}^2$) in order to minimize any spurious pressure gradients and convection effects within the cavity. Also, in order to capture the effect of cavity volume change on the cavity pressure change, the elasticity parameters were assumed to be $\nu_f = 0.49$ and $E = 3(1-2\nu_f)/C_{eq}$, where C_{eq} is the compressibility of the cavity fluid that may also contain trapped air [*Selvadurai and Najari*, 2015]. The system of *nonlinear partial differential equations* governing the fluid-filled cavity are as follows:

$$\left(K_D + \frac{G_D}{3}\right)\nabla(\nabla.\mathbf{u}) + G_D\nabla^2\mathbf{u} - K_D\beta_s\nabla T = \mathbf{0} \tag{6}$$

$$C_{eq}(p)\frac{\partial p}{\partial t} + \nabla.\left[-\frac{K}{\mu(T)}\nabla p\right] + \frac{\partial(\nabla.\mathbf{u})}{\partial t} - \beta_f(T)\frac{\partial T}{\partial t} = 0 \tag{7}$$

$$\rho_f(T)c_f\frac{\partial T}{\partial t} - k_{cf}\nabla^2 T = 0 \tag{8}$$

In the above formulation, the consideration of any trapped air within the fluid-filled cavity implies that the compressibility of the fluid in the sealed cavity is greater than the compressibility of de-aired water. A simplified relationship for the compressibility of an air-water mixture can be obtained from the form of the Voigt bound

$$C_{eq} = \varphi C_a + (1-\varphi)C_w \tag{9}$$

where φ is the air fraction in the fluid-air mixture (volume of air/volume of fluid-filled cavity), C_w is the compressibility of the pure fluid without air inclusions, i.e., $4.54\times10^{-10}\,\mathrm{Pa}^{-1}$ [*White*, 2011], and C_a is the compressibility of air at the temperature and pressure associated with the experiment. Alternatives to equation (9) that take into account air solubility have also been investigated [*Schuurman*, 1966; *Fredlund*, 1976; *Teunissen*, 1982; *Selvadurai and Najari*, 2015]. For nonisothermal phenomena the behavior of the air bubbles follows the ideal gas law:

$$\frac{P^a V^a}{T} = mR \tag{10}$$

where V^a is the volume of the air, P^a is the absolute pressure of the air bubble, T is the temperature in degrees Kelvin, m is the number of moles, and R is the universal gas constant. Considering variations in equation (10), we have

$$P^a\mathrm{d}V^a + V^a\mathrm{d}P^a = mR\mathrm{d}T \quad \Rightarrow\ C_a = \frac{-\frac{\mathrm{d}V^a}{V^a}}{\mathrm{d}P^a} = \frac{1}{P^a} - \frac{1}{T}\frac{\mathrm{d}T}{\mathrm{d}P^a} \tag{11}$$

The ideal gas law also determines the changes of air fraction with pressure and temperature. Assuming that the total volume of fluids within the cavity is constant during the THM experiment (i.e., $V^w + V^a$, with no movement of the air into the low-permeability rock), the air fraction equation can be rewritten as

$$\frac{P_0^a V_0^a}{T_0} = \frac{P^a V^a}{T};\ \ \varphi = \frac{V^a}{V^w + V^a} \quad \Rightarrow \quad \varphi = \frac{\frac{P_0^a}{P^a}\frac{T}{T_0}V_0^a}{V^w + V^a} = \frac{P_0^a}{P^a}\frac{T}{T_0}\varphi_0 \tag{12}$$

where P_0^a is the initial absolute air pressure, V_0^a is the initial volume of air, T_0 is the reference temperature, and φ_0 is the initial air fraction in the cavity.

From Henry's law, the weight of air that goes into solution depends on the absolute pressure of the air. Also, the rate of dissolution depends on the diffusivity rate of the air into water that is governed by Fick's law. The diffusivity rate for air in water is $2\times10^{-9}\,\mathrm{m}^2/\mathrm{s}$ at 25°C [*Cussler*, 2009]. The dissolved air fraction can contribute to the change in the compressibility of the air-water mixture if the rate at which air dissolves in the water is comparable to the rate at which the absolute pressure changes. Depending upon the rate of compression of an air-water

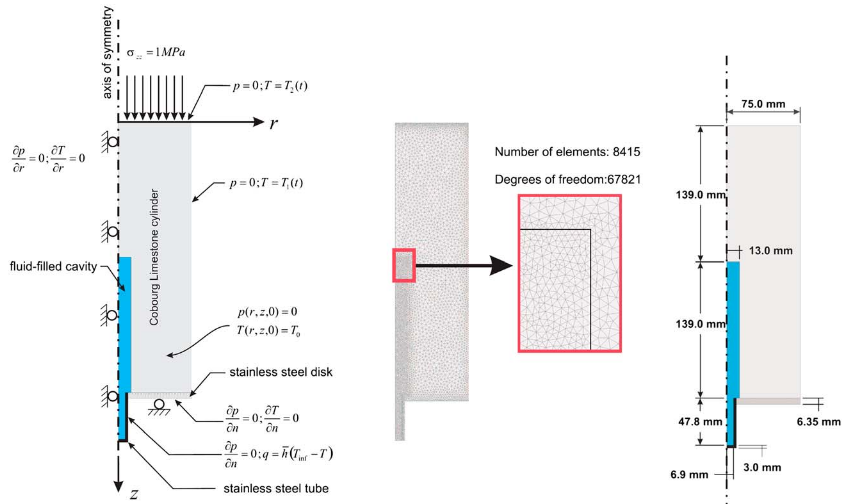

Figure 9. The boundary conditions of the thermo-hydro-mechanical problem.

mixture, the amount of air going into solution changes between 0 and $h(1-\varphi)$ of the volume of water, where h is the Henry's constant. For instance, the volume of air present in water at 25°C can be approximately 1.78% of the volume of water [*Fredlund*, 1976].

4. Computational Modeling

The THM modeling associated with this research was performed using a commercially available, general purpose multiphysics code, the accuracy of which has been established through intercode calibrations and through comparisons with analytical solutions [*Selvadurai and Najari*, 2015; *Selvadurai and Suvorov*, 2016]. This involves the finite element modeling of the coupled nonlinear partial differential equations (1) to (3) and (6) to (8) applicable to the problem domain as defined in Figure 9. The stainless steel plate epoxied to the plane surface of the Cobourg Limestone and the connected stainless steel tube were also modeled to account for all components of the experimental facility that can influence the coupled THM response of the system. The temperature boundary conditions on the cylindrical surface of the sample are specified in relation to the time history of the average surface temperatures measured at the upper, middle-height, and lower levels of the cylinder. Similarly, the boundary condition at the upper surface is the time history of the average temperatures measured at three locations on the surface. The base of the Cobourg Limestone sample, which is epoxied to the stainless steel plate, is in contact with a 3 mm thick rubber gasket. Since the thermal conductivity of the rubber material was 80 times lower than the thermal conductivity of the stainless steel, it was assumed that the plate was thermally insulated. Since the temperature on the surface of the steel tube connected to the central cavity was not controlled, a Newton cooling-type heat flux boundary condition was assumed for the cylindrical surface of the steel tube, i.e.,

$$q = \bar{h}(T_{inf} - T) \tag{13}$$

where T_{inf} is the ambient laboratory temperature and $\bar{h}$ is the heat transfer coefficient. The heat transfer coefficient depends on several factors including the geometry of the solid, the viscosity and density of the cooling fluid (in this case air), and the geometry of the space surrounding the solid. The coefficient for the free convection cooling of a solid in air varies between 10 W m^{-2} K^{-1} and 30 W m^{-2} K^{-1} [*Kakac and Yener*, 2013]. The accurate value of this parameter differs from one problem to another and should be determined through computational modeling of the specific problem using the nonisothermal form of the Navier-Stokes equations. Another method for estimating the heat transfer coefficient is through experimental investigations. In the current study, the heat transfer coefficient for the stainless steel tube connected to the central cavity was determined from the results of initial thermal tests performed on a sample of the Cobourg Limestone. A heat transfer coefficient of 16 W m^{-2} K^{-1} was obtained from the calibration of the THM model to fit the measured temperature values at the upper and lower regions of the central cavity.

Table 2. Values of the Parameters Used in the Computational Modeling of the THM Experiment

Parameter	Cobourg Limestone	Water	Stainless Steel
Young's modulus (GPa)	21[a]	-	200[b]
Poisson's ratio	0.25[a]	0.49	0.3[b]
Porosity	0.01[a]	1	-
Biot coefficient	0.7[c]	-	-
Permeability (m^2)	(6.5 to 112) × 10^{-20}	-	-
Volumetric thermal expansion coefficient (°C^{-1})	2.0 × 10^{-5}[d]	$\beta_f(T)$[e]	4.9 × 10^{-5}[b]
Thermal conductivity (W m^{-1} °C^{-1})	2.5[f]	0.58[e]	16.5[b]
Specific heat capacity (J kg^{-1} °C^{-1})	770[f]	4187[e]	480[b]

[a]*Selvadurai et al.* [2011].
[b]*McGuire* [2008].
[c]Typical value for limestone [*Wang*, 2000].
[d]*Guo* [2010].
[e]*Holzbecher* [1998].
[f]*AECL* [2011].

The typical boundary conditions and the mesh refinement associated with the computational developments of the THM testing of the Cobourg Limestone are shown in Figure 9. The graded mesh refinement for the axisymmetric THM model consists of 8415 elements and 67,821 degrees of freedom. The accuracy of the computational approach that uses either GMRES or the UMFPACK solver has been accurately verified through solution of H, HM, and THM problems [*Selvadurai and Suvorov,* 2016]. The parameters used in the computational modeling are shown in Table 2. The permeability values used in the modeling were the ones measured after performing the thermal experiments. The permeability value for each sample was estimated for both isotropic and transversely isotropic hydraulic conductivities (Table 1), as discussed in section 2.3. Isotropic elasticity and thermal properties were assumed in the computational modeling. In this study, a fully three-dimensional computational model was used to perform the THM computational simulations applicable to the transverse isotropy in sample CL-V2 where the nominal plane of stratification is aligned with the central axis of the cylindrical sample. When the nominal plane of transverse isotropy is aligned normal to the axis of the cylinder, the computational analyses were performed using a two-dimensional axisymmetric model.

The changes in pressure in the fluid-filled cavity depend mainly on (i) the movement of water between the cavity and the rock due to thermally induced fluid flow gradients toward the cavity and the hydraulic potential between the rock and the pressurized cavity, (ii) the difference between the volumetric thermal expansion of the water in the cavity and the cavity itself, and (iii) the air fraction in the cavity. Taking the extreme case when the interior surface of the cavity is hydraulically sealed (i.e., there is no exchange of water between the fluid-filled cavity and the rock), an increase in cavity pressure due to a temperature increase can be estimated using basic analytical solutions. The volumetric strain induced by a temperature increase from T1 to T2 within the fluid-filled cavity can be calculated from the result

$$\varepsilon_v^T = (1-n)\int_{T_1}^{T_2}(\beta_f - \beta_s)\mathrm{d}T \tag{14}$$

where n is the porosity of the rock, β_s is the volumetric thermal expansion coefficient of the solid grains, and β_f is the volumetric thermal expansion coefficient of the fluid estimated from [*Kell*, 1967]

$$\beta_f = 4.7222\times10^{-10}T^3 - 1.0821\times10^{-7}T^2 + 1.4071\times10^{-5}T - 3.4786\times10^{-5};\quad T\in[20, 80]\,^\circ\mathrm{C} \tag{15}$$

Also, the volumetric strain induced by an increase of fluid pressure, from atmospheric pressure to P (absolute pressure), is

$$\varepsilon_v^P = \int_{P_{\mathrm{atm}}}^{P}[(\phi C_a) + (1-\phi)C_w]\mathrm{d}P \tag{16}$$

Substituting the expression for compressibility of the air and the air void content from equations (11) and (12) into equation (16) and neglecting the term dT/dP^a, we have

$$\begin{aligned}\varepsilon_v^P &= \int_{P_{\mathrm{atm}}}^{P}\left[\frac{P_{\mathrm{atm}}\phi_0}{P^2} + \left(1 - \frac{P_{\mathrm{atm}}\phi_0}{P}\right)C_w\right]\mathrm{d}P = -P_{\mathrm{atm}}\phi_0\left[\frac{1}{P} - \frac{1}{P_{\mathrm{atm}}}\right] + C_w(P - P_{\mathrm{atm}}) \\ &-P_{\mathrm{atm}}C_w\phi_0\ln\left(\frac{P}{P_{\mathrm{atm}}}\right)\end{aligned} \tag{17}$$

Table 3. An Estimation of the Upper Bound Cavity Pressure Induced by Temperature Increase

	Thermally Induced Cavity Pressure (MPa)		
Sample	From 25°C to 40°C	From 40°C to 55°C	From 55°C to 70°C
CL-H1	0.3	1.6	4.4
CL-H2	0.4	2.4	5.4
CL-V1	9.2	13.0	16.2

Considering the compatibility of volumetric strains (i.e., assuming that the volumetric strain obtained from a temperature increase (i.e., equation (14)) equals the volumetric strain in the fluid obtained from water pressure changes within the cavity (i.e., equation (17))), the cavity pressure induced by a temperature increase can be calculated. Table 3 shows the results of cavity pressure changes obtained by equating ε_v^T and ε_v^p. Since the equations do not take into account the fluid flow through the rock, the estimated values obtained using the analytical solution will correspond to an upper bound for the rise in the cavity pressure. The estimated values depend solely on the temperature range and the air void content in the cavity.

5. Discussion

The water pressure in the fluid-filled cavity and the water temperature measured at the two ends of the cavity were compared with the computational modeling results in section 2.3. The temperature at the two ends of the fluid-filled cavity follows a time history similar to the applied temperature boundary conditions. The computational modeling satisfactorily estimated the temperature changes at the two ends of the fluid-filled cavity. This observation supports the overwhelming evidence in the literature on THM problems [*Selvadurai and Suvorov*, 2016] that the time history of temperature fields in both laboratory and field studies can be accurately predicted using the heat conduction model. In this study, the observation is extended to include *fluid inclusions* that are subjected to thermal effects. As the temperature within the rock sample increases, volumetric thermal expansion occurs in both the pore water and the solid skeleton. The volumetric thermal expansion of the Cobourg Limestone is 2×10^{-5}°C^{-1}, whereas the volumetric thermal expansion value for the water changes with temperature, from 2.07×10^{-4}°C^{-1} at 20°C to 5.84×10^{-4}°C^{-1} at 70°C. Since the thermal expansion of the water is greater than that of the porous skeleton, a temperature increase induces a rise in the cavity fluid pressure. The results show that after each increase in the boundary temperature, the cavity pressure gradually increases to a maximum value and exhibits a decay as the fluid migrates through the porous medium under a gradient in the hydraulic potential. The peak cavity pressures can exhibit a change from one sample to another, based on (i) the permeability of the sample, (ii) the rate at which the temperature increases at the outer boundaries, and (iii) the air void content within the central cavity. Table 1 shows the permeability values measured before and after the THM tests and the air void content in samples CL-H1, CL-H2, and CL-V1. A comparison of the results of the cavity pressure for samples CL-H1 and CL-H2 (Figures 6 and 7), which have a similar air void content, shows that the *peak cavity pressure* for sample CL-H2 with a permeability of 6.5×10^{-20}m^2 is *almost twice* the cavity pressure measured for the sample CL-H1 with a permeability of 1.36×10^{-19} m^2. Moreover, for each sample, a 15°C temperature increase from 25°C to 40°C, from 40°C to 55°C, and from 55°C to 70°C induces different cavity pressures. The reason for this difference is that on the one hand, the volumetric thermal expansion of water is temperature dependent and increases with temperature for temperatures greater than 4°C, whereas an increase in the temperature significantly decreases the viscosity of water and therefore increases the hydraulic conductivity of the rock and the rate at which the water pressure dissipates.

The cavity fluid pressures obtained from the computational modeling show slight discrepancies with the results of the experiments, which could arise from several factors: First, the thermal damage was not directly incorporated in the THM model. Comparing the permeability values measured before and after the THM experiments, an increase ranging from 1.3 to 8.7 times the initial permeability values was observed in each sample, most likely caused by thermal damage. The thermal damage could be the result of the differential thermal expansion of the argillaceous partings and the quartzitic nodular phase. Examples of the results of thermally induced cracking in typical sedimentary and igneous rocks are provided by *Fredrich and Wong* [1986] and *Fortin et al.* [2011]. The nonisothermal Biot's formulation can be extended to include thermomechanical damage and the changes of the permeability and poroelasticity parameters with temperature. This is perhaps easier said than done, since separate companion thermomechanical experiments need to be performed to estimate the nature of anisotropic damage that can occur at the scale of the fabric and to combine such studies to examine the evolution laws for the transport phenomena. To the authors' knowledge, there is no conclusive research available in the literature on the anisotropy of these properties on Cobourg Limestone. *Nasseri and Young* [2016] tested six Cobourg Limestone specimens and observed 0 to 25% anisotropy in the measured shear velocities parallel to and along the nominal bedding plane. Second, due to the heterogeneity of the Cobourg Limestone and evidence of discontinuities in the vicinity of the argillaceous partings, the fluid flow through the rock could be through some preferred paths and regions rather than the homogenous hydraulic characteristics that were assumed in the model. In such cases, the research must also focus on the identification of preexisting defects through appeal to CT scans. The Cobourg Limestone was modeled as an isotropic material, whereas the argillaceous partings within the nodular matrix point to the possibility of anisotropy in mechanical, hydraulic, and thermal properties of the rock. Comprehensive experimental studies need to be conducted in order to characterize either the anisotropy or the transverse isotropy in Young's modulus, Poisson's ratio, permeability, and thermal conductivity of the Cobourg Limestone. However, the comparison of the cavity pressure results obtained from the modeling that assumes elastic isotropy of the mechanical behavior, transverse-isotropic modeling of fluid transport, and isotropic effective behavior of the thermal conductivity characteristics for the given geometry and boundary conditions shows that the basic assumption of isotropic hydraulic conductivity provides results that are similar to the case where the hydraulic properties display transverse isotropy consistent with $(K_H/K_V) \approx 10$. It is, however, unreasonable to draw any general conclusions with regard to this observation since in the experimental configuration, the dominant flow pattern that will result in the dissipation of the thermally induced cavity fluid pressures is in the radial direction while the flow in the axial direction at the base of the cylindrical cavity is considerably smaller. This observation is also made in the studies by *Selvadurai and Najari* [2016] in connection with isothermal investigations of permeability. Considering the nonlinearity of the THM processes and simplifying assumptions adopted in the model, it is clear that the cavity pressure results obtained from the computational modeling give a satisfactory agreement with the experimental results. Furthermore, this satisfactory agreement is achieved with the least effort in terms of material characterization that most research laboratories have access to.

6. Concluding Remarks

In this paper the THM behavior of the argillaceous Cobourg Limestone was examined using an experimental configuration that is amenable to computational modeling. The fabric of the rock contains interbedding of an argillaceous component contributing to a heterogeneity that can be regarded as nominal bedding planes. Experiments were performed on three cylindrical samples with axes either along or perpendicular to these nominal bedding planes. For each test, the temperature on the outer surface of the sample, containing a fluid-filled central cavity, was increased from 25°C to 70°C in three stages of 15°C. The thermal loading resulted in an increase in cavity pressure during each stage. The peak cavity pressures ranged between 120 kPa and 840 kPa, depending on the permeability of the samples and the amount of air voids in the fluid-filled cavity. The permeability of the samples measured before the THM experiments was between $1.56 \times 10^{-20}\,\mathrm{m}^2$ and $3.85 \times 10^{-19}\,\mathrm{m}^2$. Repeating the permeability tests after each thermal excursion showed that heating increased the permeability of the samples between 1.3 and 8.7 times; this points to the possible evolution of thermomechanical damage that enhances the permeability of the rock. The THM experiments were modeled using the nonisothermal Biot theory of poroelasticity and solved using a multiphysics code that has been adequately validated. The formulation takes into account the coupled interaction between skeletal deformation, pore water pressure, and temperature changes. The temperature dependency of the volumetric thermal expansion and the viscosity of the permeating fluid were also considered in the developments. The equations were modified to take into account the effect of air voids in the central cavity, which can influence the compressibility of the cavity fluid and affect the generation of cavity pressures resulting from the thermophysical and thermomechanical mismatch of the rock and the cavity fluid. The time history of the cavity fluid pressure is treated as the *signature of the coupled* THM *processes* in the experiment. The studies show a satisfactory agreement between the results for the cavity pressure obtained from the experiments and the results obtained from the computational modeling. The computational modeling also estimated the temperatures within the cavity, and they were in agreement with the experimental results. An upper bound for the peak cavity pressures was also estimated using an analytical approach. The solution was obtained by considering compatibility of volumetric strains in a cavity region where fluid transport into the permeable rock is suppressed. Comparing the maximum pressures obtained from the analytical solution with the experimental results, it was noted that even for a rock with a permeability as low as $6.5 \times 10^{-20}\,\mathrm{m}^2$, neglecting the permeability would result in a significant overestimation of the thermally induced water pressure. This finding is of particular interest for understanding the response of fluid-filled inclusions in repository locations proposed for storing heat-emitting waste, which could be subjected to radiogenic heating from the stored waste. The current research shows that the THM processes in the Cobourg Limestone can be estimated, reasonably accurately, using Biot's formulation extended to include nonisothermal effects. The progressive degradation of the fluid transport properties during cycles of heating is of interest even though the radiogenic heating involves a very long duration thermal pulse with no reduction over several hundred years. Extension of the studies to include a damage mechanics approach is feasible but will entail additional considerations, including the development of an extensive program of theoretical, computational, and experimental research that takes into consideration the heterogeneity of the rock, the characterization of damage (i.e., interspecies or intraspecies in the case of the Cobourg Limestone), the evolution of interspecies and intraspecies THM damage, and the relevant damage evolution laws. While such developments are possible in the context of a theoretical and computational framework, the companion set of THM experiments needed to validate the developments will be a challenging exercise. The experimental, theoretical, and computational research presented in this paper is a plausible approach that can be progressively improved by examining other novel experimental configurations.

Acknowledgments

The authors are indebted to the reviewers for their constructive comments, which led to significant improvements in the presentation of the research. The work described in this paper was supported by a Discovery Research Grant awarded by the Natural Sciences and Engineering Research Council of Canada and research support from the Nuclear Waste Management Organization (NWMO) of Ontario, Canada, awarded to the first author. The authors are grateful to Tom Lam and Mark Jensen of NWMO for their support and valuable suggestions. The SEM Images of the Cobourg Limestone were obtained by Postdoctoral Fellow Jean-Baptiste Regnet, using the facilities at the Laboratoire de Géologie, ENS Paris. Further information on the Cobourg Limestone can be found in the KCL Web Site: https://www.mcgill.ca/civil/people/selvadurai/kcl-project. The authors are grateful to ENS for this assistance. The names of the equipment and computational platforms used in the research are omitted to ensure that there is no evidence of endorsement for the use of any equipment or software. Details of the equipment can be obtained, however, by contacting the authors. A.P.S. Selvadurai is William Scott Professor and a James McGill Professor, and M. Najari is a Former Postdoctoral Fellow.

References

AECL (2011), Internal Memorandum from Atomic Energy of Canada Limited to the Nuclear Waste Management Organization, File 22886.009080.0033.

Baud, P., A. Schubnel, and T.-F. Wong (2000), Dilatancy, compaction, and failure mode in Solenhofen Limestone, *J. Geophys. Res.*, *115*, 19,289–19,303, doi:10.1029/2000JB900133.

Biot, M. A. (1941), General theory of three-dimensional consolidation, *J. Appl. Phys.*, *12*(2), 155–164.

Carslaw, H. S., and J. C. Jaeger (1959), *Conduction of Heat in Solids*, 526 pp., Oxford Sci. Publ., Oxford.

Christensen, R. M. (1979), *Mechanics of Composite Materials*, 348 pp., John Wiley, New York.

Cussler, E. L. (2009), *Diffusion: Mass Transfer in Fluid Systems*, pp. 117–161, Cambridge Univ. Press, Cambridge.

Farmer, I. W. (1968), *Engineering Properties of Rocks*, 180 pp., E. & F.N. Spon Ltd, London.

Fortin, J., S. Stanchits, S. Vinciguerra, and Y. Gueguen (2011), Influence of thermal and mechanical cracks on permeability and elastic wave velocities in a basalt from Mt. Etna volcano subjected to elevated pressure, *Tectonophysics*, *503*, 60–74.

Fredlund, D. G. (1976), Density and compressibility characteristics of air-water mixtures, *Can. Geotech. J.*, *13*, 386–396.

Fredrich, J. T., and T.-F. Wong (1986), Micromechanics of thermally induced cracking in three crustal rocks, *J. Geophys. Res.*, *91*, 12,743–12,764, doi:10.1029/JB091iB12p12743.

Gartner Lee Limited (2008), DGR Supporting Technical Report: Phase I Geosynthesis, Report to Ontario Power Generation, 00216-REP-01300-00010-R00 (DOC 556).

Guo, R. (2010), Coupled Thermal-Mechanical Modelling of a Deep Geological Repository using the Horizontal Tunnel Placement Method in Sedimentary Rock using CODE_BRIGHT, *Nucl. Waste Manage. Organ. Tech. Rep. TR-2010-22*.

Hashin, Z., and S. Shtrikman (1963), A variational approach to the elastic behavior of multiphase minerals, *J. Mech. Phys. Solids*, *11*, 127–140.

Holzbecher, E. O. (1998), *Modelling Density-Driven Flow in Porous Media: Principles, Numerics, Software*, 286 pp., Springer, Berlin.

Jaeger, C. (1972), *Rock Mechanics and Engineering*, 417 pp., Cambridge Univ. Press, Cambridge.

Jaeger, J. C. (1965), *Elasticity, Fracture and Flow: With Engineering and Geological Applications*, 212 pp., John Wiley, New York.

Kakac, S., and Y. Yener (2013), *Convective Heat Transfer*, 622 pp., CRC Press, New York.

Kell, G. S. (1967), Precise representation of volume properties of water at one atmosphere, *J. Chem. Eng. Data*, *12*(1), 66–69.

Mazurek, M. (2004), Long-term used nuclear fuel waste management—Geoscientific review of the sedimentary sequence in Southern Ontario, *Tech. Rep. TR 04-01*, Inst. of Geol. Sci., Univ. of Bern, Switzerland.

McGuire, M. F. (2008), *Stainless Steels for Design Engineers*, 225 pp., ASM Int., Chicago.

McTigue, D. F. (1990), Flow to a heated borehole in porous, thermoelastic rock: Analysis, *Water Resour. Res.*, *26*, 1763–1774, doi:10.1029/WR026i008p01763.

Nadai, A. (1963), *Theory of Flow and Fracture of Solids*, vol. 2, 691 pp., McGraw-Hill, New York.

Nasseri, M. H. B., and R. P. Young (2016), Laboratory triaxial and permeability tests on Tournemire Shale and Cobourg Limestone: Report, Univ. of Toronto.

Neuzil, C. E. (2011), Hydromechanical effects of continental glaciation on groundwater systems, *Geofluids*, *12*, 22–37.

Neuzil, C. E., and A. M. Provost (2014), Ice sheet load cycling and fluid under pressures in the eastern Michigan Basin, Ontario, Canada, *J. Geophys. Res. Solid Earth*, *119*, 8748–8769, doi:10.1002/2014JB011643.

Nicolas, A., J. Fortin, J. B. Regnet, A. Dimanov, and Y. Gueguen (2016), Brittle and semi-brittle behaviours of a carbonate rock: Influence of water and temperature, *Geophys. J. Int.*, *206*, 438–456.

Nield, D. A., and A. Bejan (2006), *Convection in Porous Media*, 640 pp., Springer, Berlin.

Ontario Power Generation (OPG) (2008), Ontario Power Generation's Deep Geologic Repository for Low and Intermediate Level Waste, Supporting Technical Report: Phase 1-Geosynthesis, OPG 00216-REP-01300-00010-R00.

Rehbinder, G. (1995), Analytical solutions of stationary coupled thermo-hydro-mechanical problems, *Int. J. Rock Mech. Min. Sci.*, *32*, 453–463.

Rutqvist, J., Y.-S. Wu, C.-F. Tsang, and G. Bodvarsson (2002), A modeling approach for analysis of coupled multiphase fluid flow, heat transfer, and deformation in fractured porous rock, *Int. J. Rock Mech. Min. Sci.*, *39*, 429–442.

Rutqvist, J., M. Chijimatsu, L. Jing, A. Millard, T. S. Nguyen, A. Rejeb, Y. Sugita, and C.-F. Tsang (2005), Numerical study of the THM effects on the near-field safety of a hypothetical nuclear waste repository—BMT1 of the DECOVALEX III project. Part 3: Effects of THM coupling in fractured rock, *Int. J. Rock Mech. Min. Sci.*, *42*, 745–755.
Rutter, E. H. (1974), The influence of temperature, strain rate and interstitial water in the experimental deformation of calcite rocks, *Tectonophysics*, *22*, 311–334.
Schuurman, I. E. (1966), The compressibility of an air-water mixture and a theoretical relation between the air and water pressures, *Geotechnique*, *16*, 269–281.
Selvadurai, A. P. S. (2009), Influence of residual hydraulic gradients on decay curves for one-dimensional hydraulic pulse tests, *Geophys. J. Int.*, *177*, 1357–1365.
Selvadurai, A. P. S., and L. Jenner (2013), Radial flow permeability testing of an argillaceous limestone, *Ground Water*, *51*, 100–107.
Selvadurai, A. P. S., and M. Najari (2015), Laboratory-scale hydraulic pulse testing: Influence of air fraction in the fluid-filled cavity in the estimation of permeability, *Geotechnique*, *65*, 124–134.
Selvadurai, A. P. S., and M. Najari (2016), Isothermal permeability of the Argillaceous Cobourg Limestone, *Oil Gas Sci. Technol.*, *71*(4), 16, doi:10.2516/ogst/2015039.
Selvadurai, A. P. S., and T. S. Nguyen (1995), Computational modeling of isothermal consolidation of fractured porous media, *Comput. Geotech.*, *17*, 39–73.
Selvadurai, A. P. S., and A. P. Suvorov (2016), *Thermo-Poroelasticity and Geomechanics*, 264 pp., Cambridge Univ. Press, Cambridge, U. K.
Selvadurai, A. P. S., A. Letendre, and B. Hekimi (2011), Axial flow hydraulic pulse testing of an argillaceous limestone, *Environ. Earth Sci.*, *64*, 2047–2085, doi:10.1007/s12665-011-1027-7.
Teunissen, J. A. M. (1982), Mechanics of a fluid-gas mixture in a porous medium, *Mech. Mater.*, *1*, 229–237.
Tong, F., L. Jing, and R. W. Zimmerman (2010), A fully coupled thermo-hydro-mechanical model for simulating multiphase flow, deformation and heat transfer in buffer material and rock masses, *Int. J. Rock Mech. Min. Sci.*, *47*, 205–2017.
Tsang, Y. W., J. T. Birkholzer, and S. Mukhopadhyay (2009), Modeling of thermally driven hydrological processes in partially saturated fractured rock, *Rev. Geophys.*, *47*, RG3004, doi:10.1029/2008RG000265.
Vajdova, V., P. Baud, and T.-F. Wong (2004), Compaction, dilatancy and failure in porous carbonate rocks, *J. Geophys. Res.*, *109*, B05204, doi:10.1029/2003JB002508.
Vilks, P., and N. H. Miller (2007), *Evaluation of Experimental Protocols for Characterizing Diffusion in Sedimentary Rocks, Nuclear Waste Management Division Rep., TR-2007-11*, 60 pp., Atomic Energy of Canada Limited, Toronto, Ontario.
Wang, H. F. (2000), *Theory of Linear Poroelasticity With Applications to Geomechanics and Hydrogeology*, 304 pp., Princeton Univ. Press, Princeton.
White, F. M. (2011), *Fluid Mechanics*, 862 pp., McGraw-Hill, New York.
Zang, A., and O. Stephansson (2010), *Stress Field of the Earth's Crust*, 322 pp., Springer, Berlin.
Zimmerman, R. W. (2000), Coupling in poroelasticity and thermoelasticity, *Int. J. Rock Mech. Min. Sci.*, *37*, 79–87.